Deep learning and automatic reference label harvesting for Sentinel-1 SAR-based rapid tropical dry forest disturbance mapping

Adugna Mullissa [a,b,c,*], Johannes Reiche [a], Martin Herold [a,d]

[a] *Wageningen University, Droevendaalsesteeg 4, Wageningen, 6708 PB, the Netherlands*
[b] *Ctrees.org, 12 S Raymond Avenue, Pasadena, CA 91105, USA*
[c] *University of California, Los Angeles, 405 Hilgard Avenue, Los Angeles, CA 90095, USA*
[d] *Helmholtz-GeoResearch Zentrum (GFZ), Telegrafenberg, Potsdam, Germany*

ARTICLE INFO

ABSTRACT

The advent of temporally dense radar data such as the Sentinel-1 SAR have opened the door for rapid forest disturbance detection in the humid tropics. Tropical dry forest disturbance detection, however, were challenged by seasonality and more open canopy characteristics. In this manuscript, we proposed a Sentinel-1 SAR and deep learning based rapid forest disturbance detection approach for tropical dry forests. We demonstrated a weakly supervised method for reference label harvesting based on medium resolution globally available forest and forest disturbance maps. We trained a deep neural network model to derive forest and forest disturbance probabilities from Sentinel-1 images in the first step. We then implemented a probabilistic disturbance detection and refinement method to map forest disturbances in near real-time in two test regions in Paraguay and Mozambique. We mapped new forest disturbances in an emulated near real-time scenario for 2020 and 2021 and evaluated the spatial accuracy of the disturbance alerts by generating area adjusted precision, recall and F-1 score. We also evaluated the improvement in timeliness of disturbance detection by estimating mean time difference of disturbance events detection with that of Landsat-based GLAD alerts. The generated alerts in Paraguay and Mozambique achieved a precision, recall and F-1 score of 0.99, 0.61, 0.75 and 0.97, 0.51, 0.66, respectively. The proposed method detected disturbances with a mean of 21 days ($\pm$ 18 days) earlier in Paraguay and 18 days ($\pm$ 18 days) earlier in Mozambique than the Landsat-based GLAD alerts. These results demonstrated the efficacy of the proposed method and its viability to be used in an operational setting to generate large area rapid near real-time disturbance alerts in the dry tropics.

1. Introduction

Tropical dry forests (TDFs) cover approximately 40% of the globally available tropical forest stock (Murphy and Lugo, 1995; Miles et al., 2006); they play an essential role in the global carbon and water cycle and provide major ecosystem and societal services (Lewis et al., 2009; Zhou et al., 2013). In tropical regions, most of the change associated with TDFs is due to anthropogenic disturbances driven by agriculture, mining and urban expansions that results in degradation, biodiversity loss, loss of biomass and green house gas emissions (Pearson et al., 2017). There is a strong need to persistently monitor changes in TDFs to support sustainable land management and law enforcement activities to reduce illegal deforestation (Janzen, 1988; Miles et al., 2006; Portillo-Quintero and Sánchez-Azofeifa, 2010).

Satellite-based monitoring is the main technology for deriving spatially explicit near real-time (NRT) detection of forest disturbances (Reiche et al., 2018). NRT forest disturbance alerting systems aim to detect new disturbances in forests as soon as new satellite images become available (Reiche et al., 2015a). The potential of NRT systems to support policy-making and law enforcement has been widely discussed and demonstrated (Assunção et al., 2013; Lynch et al., 2013; Wheeler et al., 2014; Hansen et al., 2016; Reiche et al., 2021).

Currently, most NRT tropical forest disturbance alert systems rely on optical satellite images. The major limitation of optical satellite images in NRT systems is the late and/or missed detection of disturbances due to pervasive cloud cover, in particular during the rainy season (Reiche et al., 2018; Hansen et al., 2016; Souza et al., 2013; Sannier et al., 2014; Reiche et al., 2015b). SAR satellite images offer a better prospect, as they

---

operate in almost all weather conditions, day and night. Therefore, they have the potential to complement optical-based forest monitoring systems (De Sy et al., 2012; Joshi et al., 2016; Laurin et al., 2013). In this regard, the launch of the Sentinel-1 A and —1B C-band SAR satellites (Torres et al., 2012) and the associated open data policy from the European Space Agency open up unprecedented opportunities to provide NRT forest disturbance detection over the tropics by utilizing images consistently acquired every 6–12 days (Reiche et al., 2021).

A good demonstration of these capabilities is the Radar for Detecting Deforestation (RADD) alert system (Reiche et al., 2021), a NRT tropical humid forest (THF) disturbance detection system operating across the pan-tropics. The RADD alerts (Reiche et al., 2021), operated by Wageningen University in the Netherlands, flagged potential disturbance by comparing the most recent Sentinel-1 image with the historical stable forest descriptors. They also implemented a Bayesian updating approach to derive the conditional probabilities of forest disturbance. Subsequent observations were used to update the probability of forest disturbance (increase confidence), and to establish a user set thresholds and temporal windows to determine which of the flags were credible high-confidence alerts and which were false alarms.

Other notable wide-area forest disturbance alerts utilizing Sentinel-1C-band SAR data include the methodology by the French Centre d'Etudes Spatiales de la Biosphère (CESBIO) (Bouvet et al., 2018), DETER-R (Doblas et al., 2022) and wide-area forest degradation and deforestation monitoring proposed by (Hoekman et al., 2020). Other than Sentinel-1 SAR, the JJ-FAST alert system has been developed by the Japanese Space Agency JAXA and is based on an L-band SAR data from ALOS-PALSAR and PALSAR2 ScanSAR data (Rosenqvist et al., 2004). A detailed summary and comparison of the alert systems is provided in (Doblas Prieto et al., 2023).

Despite its early detection capabilities, the SAR-based alerts has mainly been used over THFs and their efficacy over TDFs was largely undetermined (Reiche et al., 2018). Therefore, expanding the THF NRT disturbance detection capability from THFs to TDFs was of paramount importance. To this end, a number of key challenges were defined as to why appropriate systems utilizing SAR data for NRT TDF disturbance detection and alerting have been limited to small test sites.

The first challenge of using SAR images for NRT monitoring of TDFs disturbance was the backscatter variation due to seasonality. Detecting disturbance in satellite image time-series in TDF requires the compensation of the seasonal forest component. Otherwise, the seasonal variations may lead to substantial false detection of forest disturbance (Hamunyela et al., 2016). The seasonal forest component in the SAR time-series signal was driven by changes in canopy structure and moisture that cause seasonal variations in the SAR backscatter signal (Ulaby et al., 1986). In time-series change detection, the seasonal forest component was often compensated by seasonal model fitting to account for forest seasonality (Verbesselt et al., 2010; Zhu et al., 2012). However, shifts in seasons affected the seasonality mitigation step, which caused imprecision's in the removal of the seasonal component of the signal. Some attempts have been made to mitigate the seasonality without the dependency on dense time-series images by spatial image normalization (Hamunyela et al., 2016). Each pixel was normalized with the value of dense forest in the spatial surrounding of the pixel to be normalized. The efficacy of spatial image normalization in optical images and SAR images was shown in (Reiche et al., 2018; Hamunyela et al., 2016; Watanabe et al., 2021).

The second challenge for NRT monitoring of TDF disturbance was the variation in the structure and canopy cover in different eco-regions over time (Verhegghen et al., 2022). As opposed to a THF, a TDF consisted of open canopy cover and there existed significant herbaceous under-story that complicated disturbance detection. For optical-based monitoring systems, this along with seasonality effect posed a challenge for NRT monitoring of TDF (Fig. 1). However, C-Band radar data from Sentinel-1 satellites were less affected by seasonality as compared with optical images as the backscatter was confined from the top of the

canopy and backscatter variation between the dry and wet season was small (Fig. 1).

Recently, with the proliferation of data driven approaches, machine learning was increasingly used to detect forest disturbances in THF's (Liu et al., 2018; Chen et al., 2021). Recent advances in advanced machine learning approaches provided the opportunity to mitigate the seasonality effect and the disparity in canopy structure in time-series data with the caveat of manually curating reference datasets (Solórzano and Gao, 2022; Pacheco-Pascagaza et al., 2022). In this regard, recurrent neural networks are prominent machine learning approaches that are particularly suited for time-series data (Ye et al., 2019). LSTM (Long short term memory) and GRU (gated recurrent units) are notable variants that learned the time dependencies within the data and focused on the temporal dynamics of the time-series data by explicitly controlling the flow of information through time (Wang et al., 2019; Zhong et al., 2019).

These approaches could be used to implicitly learn the seasonal patterns of TDFs to detect changes (Mullissa et al., 2023). However, time-series based neural networks for NRT disturbance detection was computationally expensive as the whole time-series needed to be processed every time a new image acquisition became available. To mitigate this limitation, robust time-series feature engineering (Zheng and Casari, 2018) coupled with standard deep neural networks (DNNs) or convolution neural networks (CNNs) offered the potential to make TDF disturbance prediction on an image to image basis. Therefore, it was imperative to engineer features that represented the temporal dynamics of the time-series to train a TDF disturbance detection model that predicted disturbance as newly acquired images became available. CNNs were more suitable to learn features that had complex spatial-contextual relationships such as landcover mapping with the caveat of computational complexity (Wang et al., 2018; Liu et al., 2019). For SAR-based forest mapping, where the requirement for complex spatial-contextual feature learning was not as important, spatial-contextual feature extractors of CNNs could be replaced with computationally cheap pixel based dense neurons, as found in deep neural network (DNN).

One of the main challenges in employing these approaches was the lack of high quality reference data needed to train these models. As ground-based reference data on TDF disturbances were very rare and manual annotation of reference data was time consuming and expensive, a weakly supervised approach could be adopted. Weak supervision is a set of machine learning approaches that use higher level and often noisier labels to synthesize a large quantity of reference labels by iterative refinement (Zhou, 2018). These techniques involve incomplete supervision i.e. when the available reference labels are precise but few in number to train a high quality model and there exists sufficient supply of unlabeled data (Wang et al., 2020). These categories encompass the fields of active learning and self-supervised learning. The second category involves inexact supervision i.e. the labeling is coarse or high level such as image level annotations and the required labels for the task are pixel level (Wei et al., 2016; Huang et al., 2018; Ahn and Kwak, 2018). The third type of weak supervision is inaccurate supervision, indicating the reference labels are public or crowd-sourced datasets that are noisy; therefore, the labels are iteratively refined to a high quality reference data (Daudt et al., 2019). In this manuscript, we used a weakly supervised approach that aligned with inaccurate supervision that iteratively upgraded the quality of existing noisy reference datasets. In this regard, globally available forest change maps (e.g. Landsat-based GLAD alerts (Hansen et al., 2016), annual Landsat-based Hansen Global Forest Change dataset (Hansen et al., 2013)) were used as noisy labels in the weakly supervised framework.

In SAR-based NRT forest disturbance monitoring, most methods in the literature were focused on THFs. As THF had dense canopy cover and less seasonality, simple machine learning models could derive high accuracies (e.g. GMM in the case of the RADD alerts). Applying simple machine learning models to TDF, however, presented a challenge, as simple parametric models may not be suitable due to seasonality and
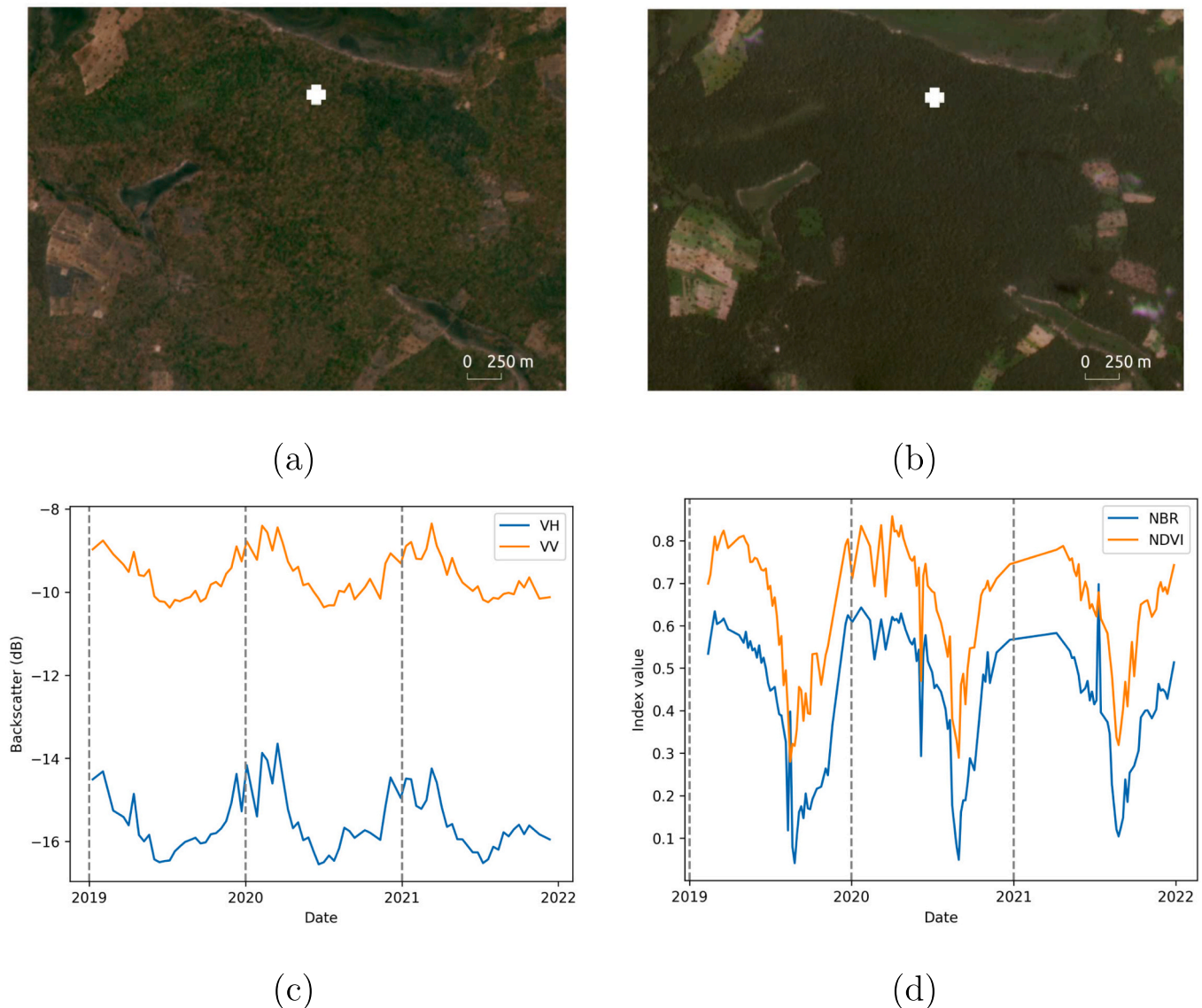
Fig. 1. The seasonality for stable dry forest in Planet Scope images (4.7 m resolution) during the (a) dry (September 2020) and (b) wet (April 2021) seasons. The corresponding time-series derived from (c) Sentinel-1 VV and VH polarization in the descending orbit and (d) Sentinel-2 normalized burn ratio (NBR) and Normalized Difference Vegetation Index (NDVI) in the Miombo woodland in Zambia (latitude:-13.17, longitude:27.64). In the Sentinel-1 SAR time-series, the variation due to seasonality is not visible in a single pixel because of speckle; therefore, we have synthesized the time series by aggregating 100 neighboring pixels (10×10 neighborhood window) whose center is indicated by the white cross in the images. The Sentinel-2 time-series, however, was synthesized without spatial aggregation as the seasonality is readily visible.

open-canopy structure. Deep learning provided a unique opportunity to solve this challenge, as it learned non-linear functions if supplied with adequate reference data. Our research addressed the application of small deep learning models to TDF disturbance detection by efficiently harvesting reference datasets without manual work at scale. Therefore, the novelty of our work was the weakly supervised deep learning approach to automatically harvest high quality reference dataset to train and predict TDF disturbances in a near real-time setting. The main objective of this manuscript was to demonstrate a Sentinel-1 SAR-based rapid forest disturbance detection system for the dry tropics. We had the following two sub-objectives:

1. Develop a weakly supervised approach that leveraged global forest loss data to generate high quality reference data.

2. Develop a deep-learning-based system for near real-time TDF disturbance alerting based on Sentinel-1 SAR data.

2. Study regions

We used two areas in Paraguay (South America) and Mozambique (Africa) to detect TDF disturbances in an NRT setting. While forest disturbance is defined in many ways, we followed a forest cover definition in a sense that pixels with less than 30% canopy cover were considered non-forest.

The first study area is located in Northern Paraguay (centred at Lat: -21.07^0, Lon: -58.77^0) (Fig. 2). We selected the province of Mariscal with an area of $72,389$ km^2 for training a deep learning model, and the province of Fuerte with an area of $19,583$ km^2 was used to test the proposed method in NRT setting. The area is found in the Dry Chaco ecoregion, characterized by tropical and subtropical grasslands, savannas and shrub-lands biome (Dinerstein et al., 2017) with a humid tropical climate with distinct wet October–May and dry seasons
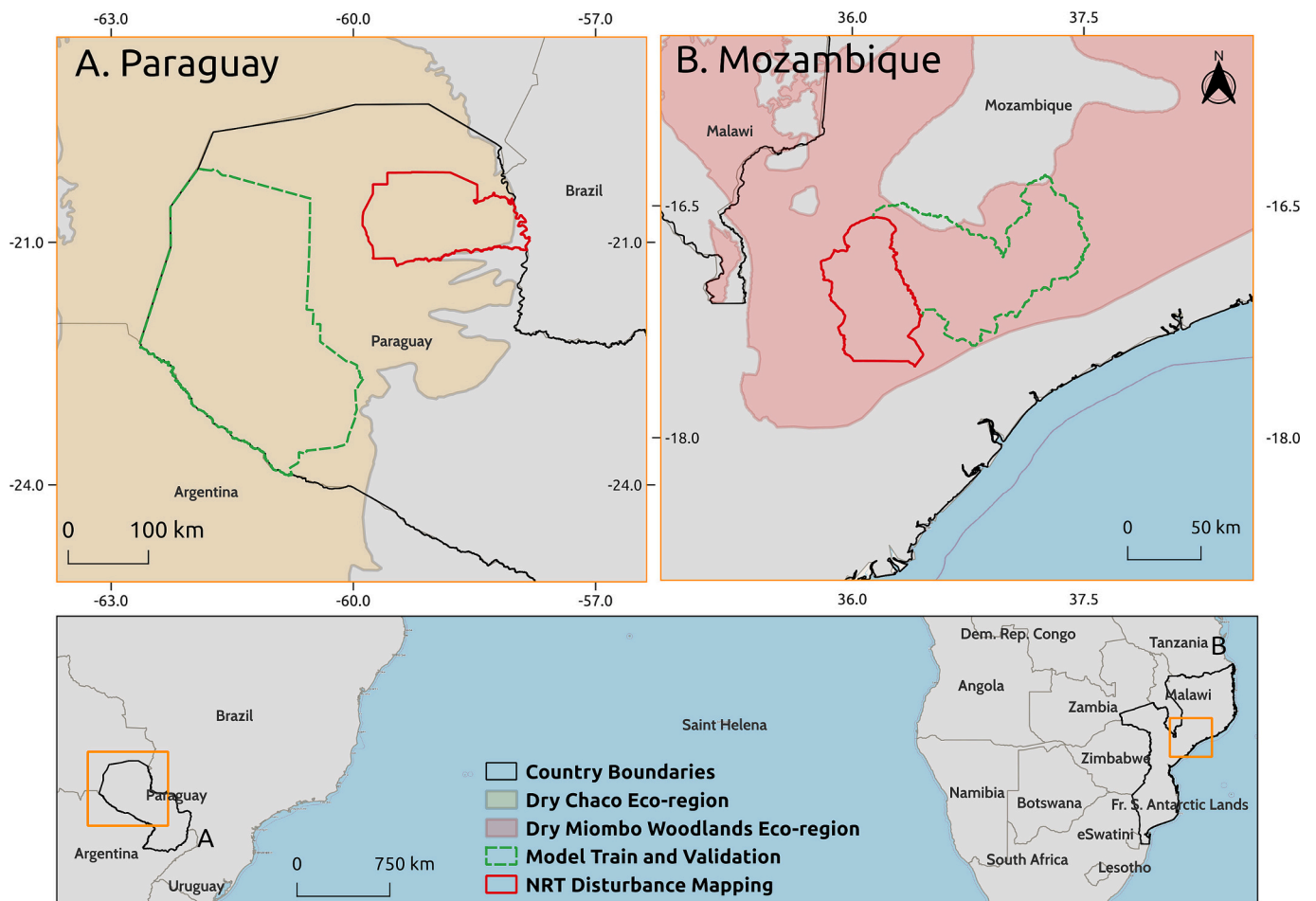
Fig. 2. Model training and validation area locations in Paraguay (A) and Mozambique (B) with the corresponding NRT disturbance mapping locations.

June–September. Forest disturbances in the area were characterized by large-scale industrial logging and agricultural expansion (Hartung et al., 2021).

The second NRT disturbance mapping area is located in the central part of Mozambique (centred at Lat: -17.09^0, Lon:36.16^0). Here, the training and NRT testing areas were selected from the province of Macuba and Derre, respectively. The training area covered $8,801$ km^2 whereas the NRT test area covered $4,762$ km^2. The areas are found within the Dry Miombo Woodlands eco-region, characterized by tropical and subtropical grasslands, savannas and shrub-lands biome with a humid tropical climate with the wet season occurring from (November–March) and the dry seasons occurring in May–October (Dinerstein et al., 2017). The change from wet and dry seasons was associated with a strong change in forest phenology, which is visible in SAR time-series. Forest disturbance in the area was mainly caused by smallholder agriculture expansion and logging activities (Nazerali and Chauque, 2023). We have selected these two areas because they represent a variety of dry forest eco-regions and drivers of forest disturbances.

The training areas indicated in Fig. 2 were used to generate the deep learning training and validation data samples. While the NRT disturbance mapping areas were used to generate the NRT TDF disturbance maps using the trained models from the training area. The NRT TDF disturbance maps were validated using an independent reference data-sets extracted from Planet images.

3. Data

3.1. Sentinel-1 SAR data

We used Sentinel-1 ground range detected SAR images in dual polarization mode (VV and VH) acquired in the respective study areas from 2018 to 2022 in Google Earth Engine (GEE) platform (Gorelick et al., 2017). The Sentinel-1 SAR images were acquired in the interferometric wide-swath mode with a resolution of 20 m by 22 m in range and azimuth directions respectively (Torres et al., 2012). The Sentinel-1 images were acquired in both ascending and descending orbits, with nominal temporal resolution of 6–12 days. Prior to their ingestion into GEE, the Sentinel-1 images were processed for thermal noise removal, calibrated to sigma nought and range Doppler terrain correction was performed. The images were available in GEE with a ground sampling distance of 10 m.

For the Paraguay test area, 408 images were acquired in ascending orbit, and 834 images were acquired in descending orbit in both the historical (i.e. the period representing stable dry forest from January 1, 2018 to December 31, 2019) and monitoring (period for monitoring TDF disturbance, January 1, 2020 to December 31, 2021) period, whereas for the Mozambique test site, we selected 737 images in the ascending orbit and 442 images in descending orbit in both the historical and monitoring period. All the images were processed in dual polarization mode.
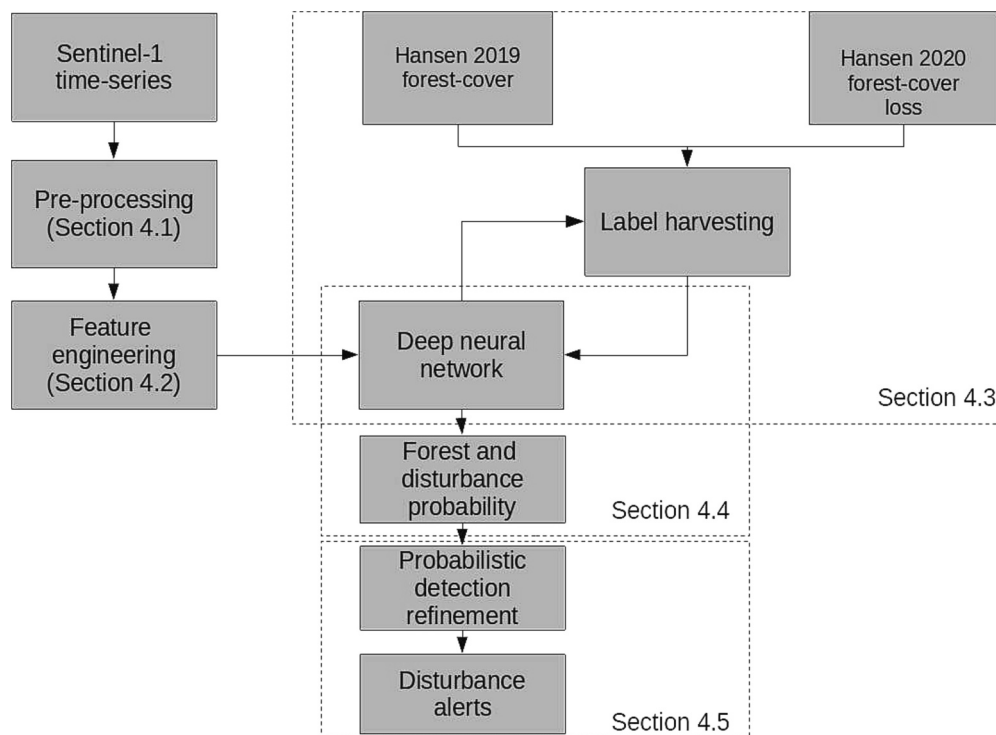
Fig. 3. The general methodological framework for the proposed TDF disturbance alerts.

3.2. Forest and forest-loss data

We used the 2020 Hansen forest-cover loss data (hereafter referred to as'Hansen 2020 forest-cover loss') (Hansen et al., 2016) to synthesize the disturbance labels. To generate the forest cover baseline map for 2019 and synthesize the forest labels, we used the Hansen 2000 forest-cover percentage map (with 30% tree cover threshold) and removed 2001–2019 Hansen forest-cover loss. We hereafter refer to the 2019 forest-cover baseline map as'Hansen 2019 forest-cover dataset'.

4. Methods

The general flowchart of the proposed approach is shown in Fig. 3. The indicated processing steps are described in the following sub-sections. We first pre-processed Sentinel-1 SAR data (Section 4.1). Secondly, we applied feature engineering (Section 4.2), followed by a reference label harvesting method (Section 4.3). Finally, we proposed to use the harvested labels to train a deep learning model to generate forest and forest disturbance probabilities (Section 4.4) that will be used in a probabilistic disturbance detection refinement method (Section 4.5) to generate alerts. The first part of the methodology was focused on iteratively refining a reference data to train a deep learning model. The model was used to derive forest and disturbance probabilities on a pixel to pixel basis. The second part of the methodology adopted the probabilistic refinement method suggested by (Reiche et al., 2018; Reiche et al., 2015a) to generate an NRT TDF disturbance alert.

4.1. SAR data pre-processing

We created Sentinel-1 SAR analysis ready data (ARD) in GEE following the methods described in (Mullissa et al., 2021). The Sentinel-1 ARD was created by applying additional border noise correction to remove remaining border artefacts in the Sentinel-1 images. We also applied multi-temporal speckle filtering using the framework suggested by (Quegan and Yu, 2001). We applied the multi-temporal filtering framework with a Lee filter (Lee, 1981) of kernel size of 9 × 9 pixels. For optimal filtered output, we have restricted the number of images

involved in the filtering to 40. Radiometric terrain normalization was also applied to mitigate the backscattered signal variation due to topography using a 1 arc-second (30 m) SRTM digital elevation model. A volume scattering model was used for the normalization (Hoekman and Reiche, 2015; Vollrath et al., 2020). This processing was performed separately for the ascending and descending orbits.

4.2. Feature engineering

We generated historical stable forest metrics that represented TDF dynamics for 2018 and 2019. The historical stable forest metrics are temporal features that best represent the dynamics of stable forests. We first removed outliers present in the Sentinel-1 image time-series using a Hampel outlier detection approach (Hampel, 1974). We discarded images with extremely low values due to rain cells from the image collection. For THFs, (Reiche et al., 2021) used the median and standard deviation to represent the signal variation, as no seasonal effects exist in THFs. In tropical South American and African dry forests, we observed that forested areas had higher backscatter values in both VV and VH polarization and lower variation in backscatter values, whereas areas with agricultural crops and bare grounds had a higher variance in the backscatter values (Verhegghen et al., 2022). When considering C-band SAR time-series it can clearly be observed that in dry seasons, even with complete loss of foliage in a forest, there was still substantial interaction with the branches. Therefore, the seasonality in Sentinel-1 time-series was not as pronounced as in optical time-series (Fig. 1). When substantial TDF disturbance happened, the scattering mechanism of the resolution cell changed from volume to surface; therefore, the backscattered signal decreased significantly especially in the VH polarization. Thus, we have chosen the median and minimum 2% of the backscatter values from both polarizations in the time-series to represent the historical stable TDF dynamics. These time-series metrics combined with individual images in the monitoring period (a time period where disturbance detections are conducted) were used to train a deep neural network to detect TDF disturbances in a before and after disturbance scenario.
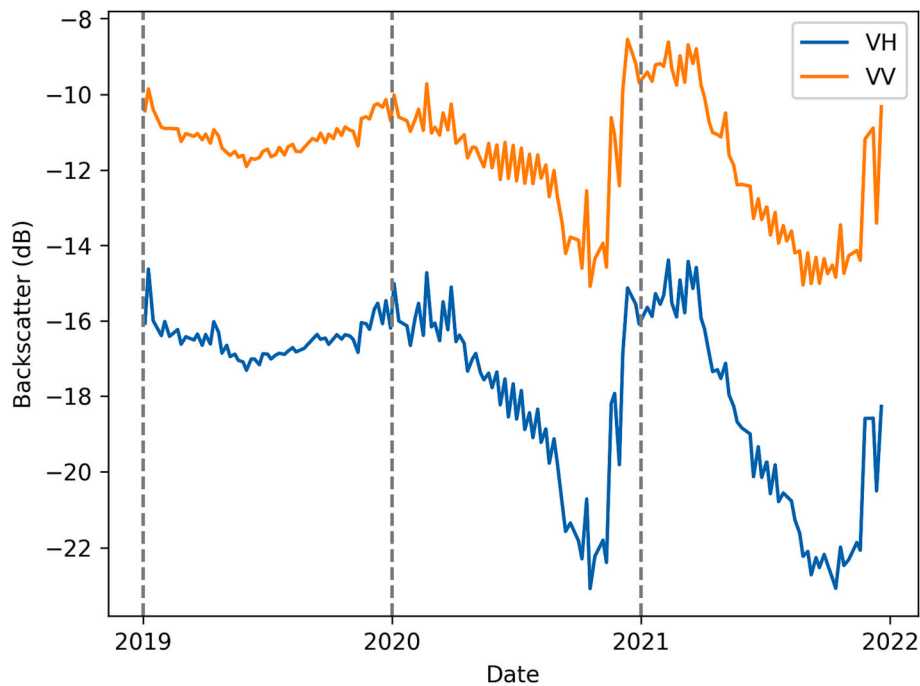
Fig. 4. A time-series of Sentinel-1 backscatter values in dB scale. The series clearly shows TDF disturbance in August 2020. The series also shows the post disturbance signal dynamics in early 2021.

4.3. Reference label harvesting

4.3.1. Forest disturbance label selection

We adopted a weakly supervised approach to synthesize the disturbance reference labels by iteratively refining an initial selection of noisy forest disturbance data collected from globally available Hansen 2020 forest-cover loss dataset (Hansen et al., 2016). The Hansen annual forest-cover loss data were produced from annual cloud-free Landsat composites, which comprised forest-cover loss accumulated for an entire year. It did not provide information on when the disturbance was detected. This made it challenging to correspond these data to a specific image in the Sentinel-1 image collection. This challenge was especially prominent for forest disturbance occurring earlier in the year where there was some re-growth in the under-story by the end of the year. In
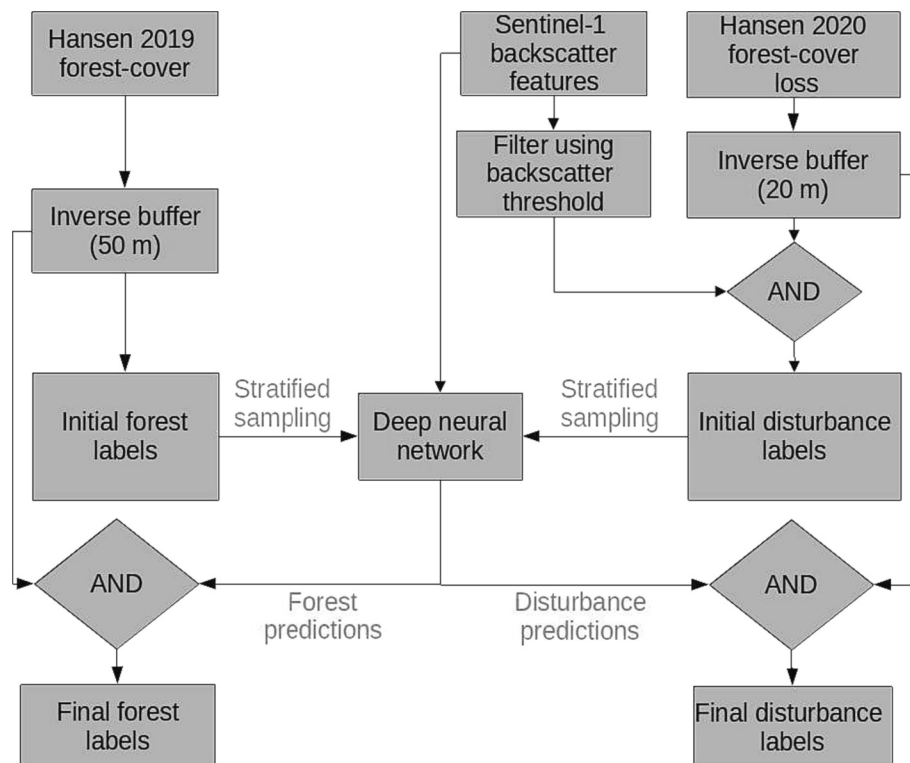

Fig. 5. Weakly supervised reference label harvesting workflow. The AND condition indicates the agreement between the indicated datasets.
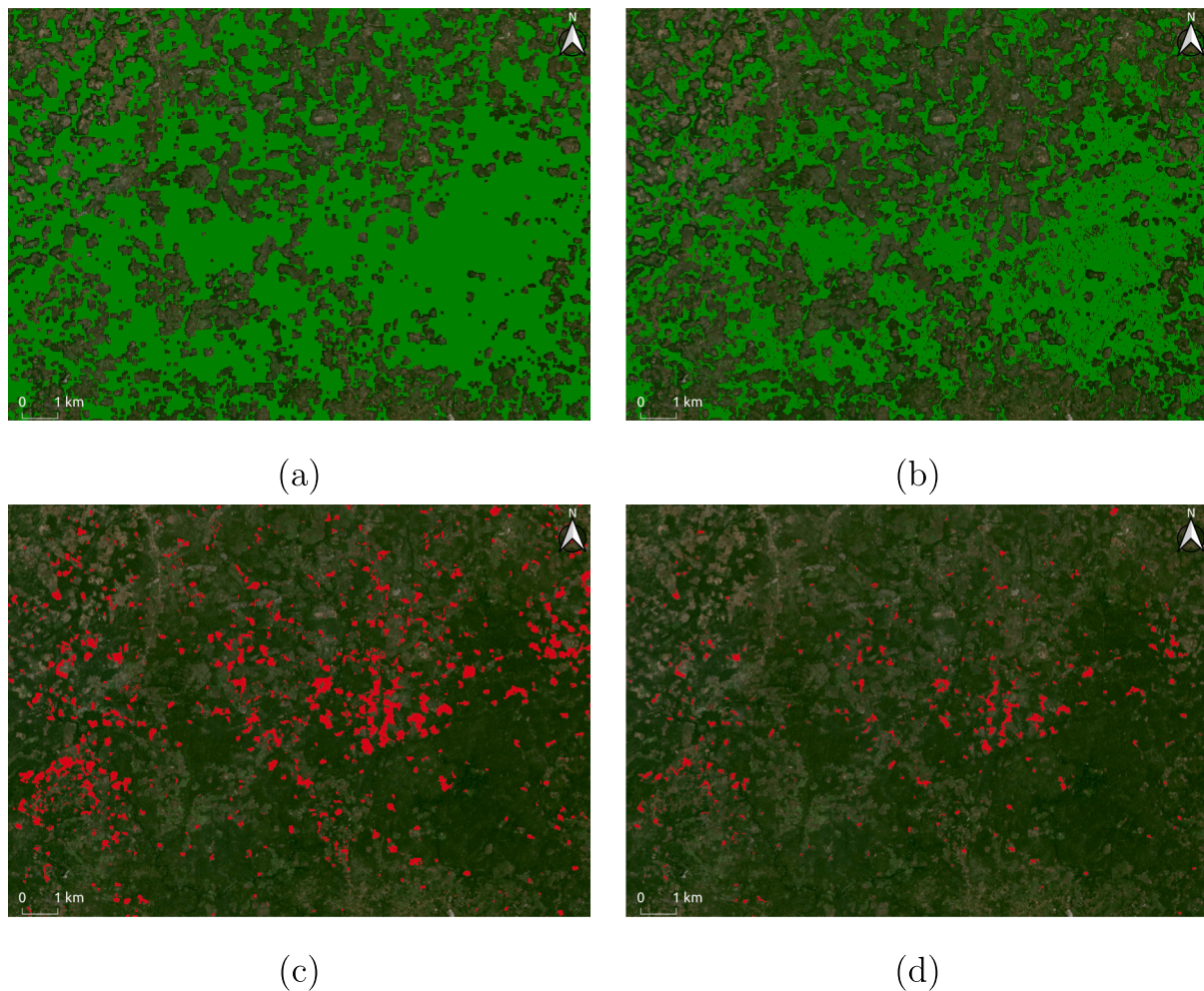
Fig. 6. Label harvesting in the Mozambique training site. (a) Hansen 2019 forest cover (unrefined forest labels). (b) Harvested stable forest labels. (c) Hansen 2020 forest loss (Unrefined forest disturbnce labels). (d) Harvested disturbance labels corresponding with Sentinel-1 image acquired on December 9, 2020 in ascending orbit. Scene center coordinate (latitude: -16.82^0, longitude: 36.40^0).

those cases, the backscatter in pixels containing regrowth was identical to that of a stable forest pixel. In addition, the Hansen forest-cover loss data were processed from Landsat at 30 m ground sampling distance and the forest loss pixels may not exactly have matched with the 10 m Sentinel-1 image, thus introducing noise in the label. Therefore, we refined the Hansen 2020 forest-cover loss to match with Sentinel-1 images from December 1 to December 31, 2020 and used them as initial forest disturbance labels. We accomplished this by spatially selecting the forest loss pixels that intersected with pixels below a user set threshold of the VH and VV backscatter values for each individual Sentinel-1 image acquired between December 1 and December 31, 2020 (Fig. 5). Here, we processed the ascending and descending orbits separately. This threshold value was determined empirically by comparing the histogram of pixels intersecting with the Hansen 2020 forest-cover loss data and the image histogram. This step was crucial as it helped to reject labels intersecting with regrowth or some forest pixels found between deforested land as found in large scale industrial logging operations in South America. To remove the edge pixel effect, we applied an inverse buffer of 20 m at Sentinel-1 image scale to all selected initial forest loss plots.

The selected initial labels were used to train a DNN (Section 4.4) model to make a forest and disturbance prediction. We selected the specific DNN architecture to minimize the computational complexity while maintaining model accuracy during prediction. During prediction, we used a probability threshold of 70% to extract the disturbance pixels

and 70% to select the stable forest pixels. The final disturbance labels were selected from the intersection between the Hansen 2020 forest-cover loss data and the disturbance prediction from the initial DNN model within the time period of December 1, 2020 to December 31, 2020 (Fig. 6). These final reference labels were used to train the final DNN model that will be used to predict the forest mask in the NRT disturbance mapping area and generate the NRT TDF disturbance alerts.

4.3.2. Stable forest label selection

To select the labels for a stable forest, we removed the Hansen 2020 forest-cover loss from the Hansen 2019 forest-cover map. We selected the initial stable TDF reference labels by applying an inverse buffer of 50 m from the data layer. The forest mask that will be used in the NRT alerts was predicted using the probability of forest generated at prediction time using the engineered features at the start of the monitoring period in the test regions. The probability of disturbance for each image in the monitoring period was used to generate the NRT TDF disturbance alerts.

4.3.3. Training sample selection

We added the median and 2% minimum of the historical period (i.e. from January 1, 2018 to December 31, 2019), as bands to images in the sampling period (December 1 to December 31, 2020) so the input feature vector represented a 1×3 feature vector for each polarization state. First, the initial TDF and disturbance labels were prepared as input
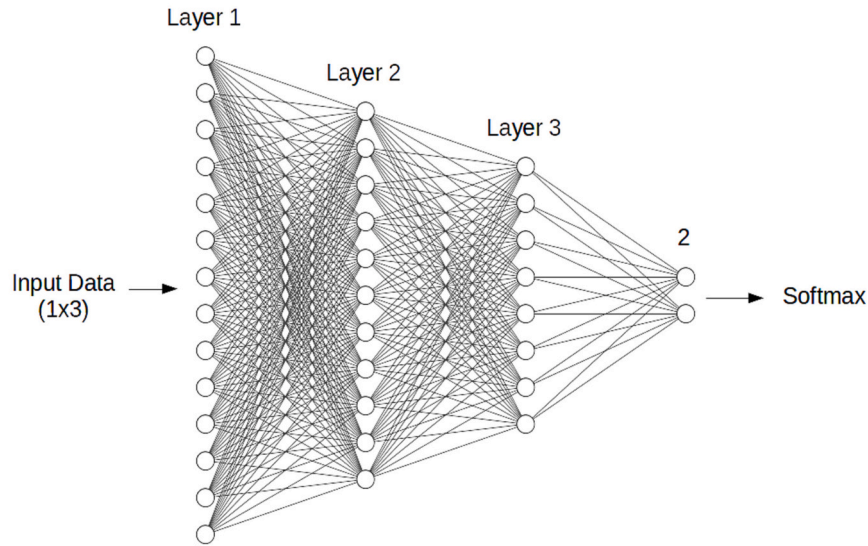
Fig. 7. The deep neural network architecture used by the proposed method for the VV or VH polarization. The input data dimension (1×3) indicated the input features i.e. backscatter image pixel from a single date in the monitoring period, the median and 2% minimum image pixels from the historical period. We trained two separate models for the VV or VH polarizations. ReLU, Rectified Linear Unit.

training data by stratified random sampling of 20,000 pixels (10,000 pixels for TDF and 10,000 samples for the disturbance class). We used the 20,000 label pixels to sample the Sentinel-1 VV and VH polarization images acquired during the sampling period (December 1 to December 31, 2020) separately in ascending and descending orbits. The sampled data consisted of 52,615 and 103,728 samples over Paraguay and 51,900 and 40,623 samples over Mozambique in the designated sampling regions for the VV and VH polarizations respectively (Fig. 2). The synthesized dataset was randomly split into 80% training data, 10% validation data and 10% test data. We have not, however, used the testing samples to test model accuracy as they were biased by label harvesting (Section 4.3.)

4.4. Deep neural network

We trained separate models for Paraguay and Mozambique in the VV and VH polarization to accommodate the variability in the TDF seasonality and forest types, respectively. We selected a DNN architecture (Fig. 7) with three hidden layers interleaved with batch normalization (Ioffe and Szegedy, 2015) and Rectified Linear Unit (ReLU) activation and Dropout layers. We used TensorFlow 2.8 (Abadi et al., 2016) to train the model, using the Adam optimizer (Kingma and Ba, 2014) with a batch size of 32 and a categorical cross-entropy loss function. We trained the model for 50 epochs. We applied hyper-parameter tuning using the Keras tuner package (O'Malley et al., 2019) using Hyperband tuner (Li et al., 2017), to select the optimal number of neurons for each hidden layer and the optimal learning rate. The optimal number of units and trainable parameters in the DNN is shown in Table 1. The optimal learning rate for both VV and VH polarization was 0.001.

The final DNN models corresponding with the VV and VH

Table 1
The number of units in each hidden layer and trainable parameters in the DNN architecture used to train the model in the respective study areas.

Region	Polarization	Layer 1	Layer 2	Layer 3	Parameters
Paraguay	VV	160	576	544	411,459
Paraguay	VH	448	896	640	984,067
Mozambique	VV	576	640	288	560,067
Mozambique	VH	224	768	128	274,755

polarization in their respective areas were used to generate forest and disturbance probabilities for each image in the monitoring period for NRT TDF disturbance mapping. These VV and VH polarization derived probabilities were fused in the probabilistic refinement step to make TDF disturbance detections.

4.5. Probabilistic detection refinement

To detect disturbances in TDF, we used the Bayesian updating approach proposed by (Reiche et al., 2018; Reiche et al., 2015a). In a near real-time monitoring scenario with past observations given as $(t - 1)$, current as (t) and future as $(t + 1)$ observations, where individual images are added to the stack chronologically as they are acquired from the start of the monitoring period on-wards, the probability of disturbance $P(D)$, derived from each pixel using the DNN model, is given as:

$$P(D) = P(D)_{XX}{}^{*} P(D)_{XY} \tag{1}$$

Here $P(D)_{XY}$ is the probability of disturbance derived from the DNN model in the XY polarization state indexed as VH. The current (t) probability of disturbance was used to detect disturbance events with low confidence when the probability of disturbance exceeds a user set threshold. For low confidence alerts, the posterior probability of forest disturbance was estimated using Bayesian updating (Reiche et al., 2015a) by taking the previous $(t - 1)$ and current (t) probability of disturbance. The Bayesian probability updating is given as:

$$P(D)_{Posterior} = \frac{P(D)_{t-1}{}^{*} P(D)_t}{P(D)_{t-1}{}^{*} P(D)_t + \left((1 - P(D)_{t-1}) * (1 - P(D)_t) \right)}. \tag{2}$$

At the beginning of the monitoring period, the $P(D)_{Posterior}$ is estimated by assuming a prior probability of zero. In subsequent acquisitions the $P(D)_{Posterior}$ is updated using the current and previous probabilities from the DNN model. The iterative Bayesian updating is stopped when TDF disturbance events are detected with high confidence i.e. when $P(D)_{Posterior}$ exceeds a predetermined threshold value χ within a given time-period. If the conditional probability of disturbance falls below χ for the low confidence alerts, or if the posterior probability fails to exceed χ within a given time, the pixel is un-selected as a disturbance event.

Fig. 8. Forest disturbance dates mapped from January 1, 2020 to December 31, 2021 for the Paraguay test area (top) and the Mozambique test area (bottom).

Table 2
Precision (user accuracy), recall (producers accuracy), F-1 score for the mapped forest disturbances for 2020 and 2021. The proposed method without label refinement followed the same procedure as the proposed method, except the deep learning model was trained using the unrefined Hansen forest-cover loss dataset.

| Region	Method	Precision (users accuracy)	Recall (producers accuracy)	F-1 score
Paraguay	Proposed method with label harvesting	0.99	0.61	0.75
Paraguay	Proposed method without label harvesting	0.88	0.13	0.22
Paraguay	Hansen forest-cover loss	0.95	0.51	0.66
Paraguay	GLAD alerts	0.93	0.23	0.36
Mozambique	Proposed method with label harvesting	0.97	0.51	0.66
Mozambique	Proposed method without label harvesting	0.88	0.16	0.26
Mozambique	Hansen forest-cover loss	0.90	0.40	0.55
Mozambique	GLAD alerts	0.59	0.06	0.10
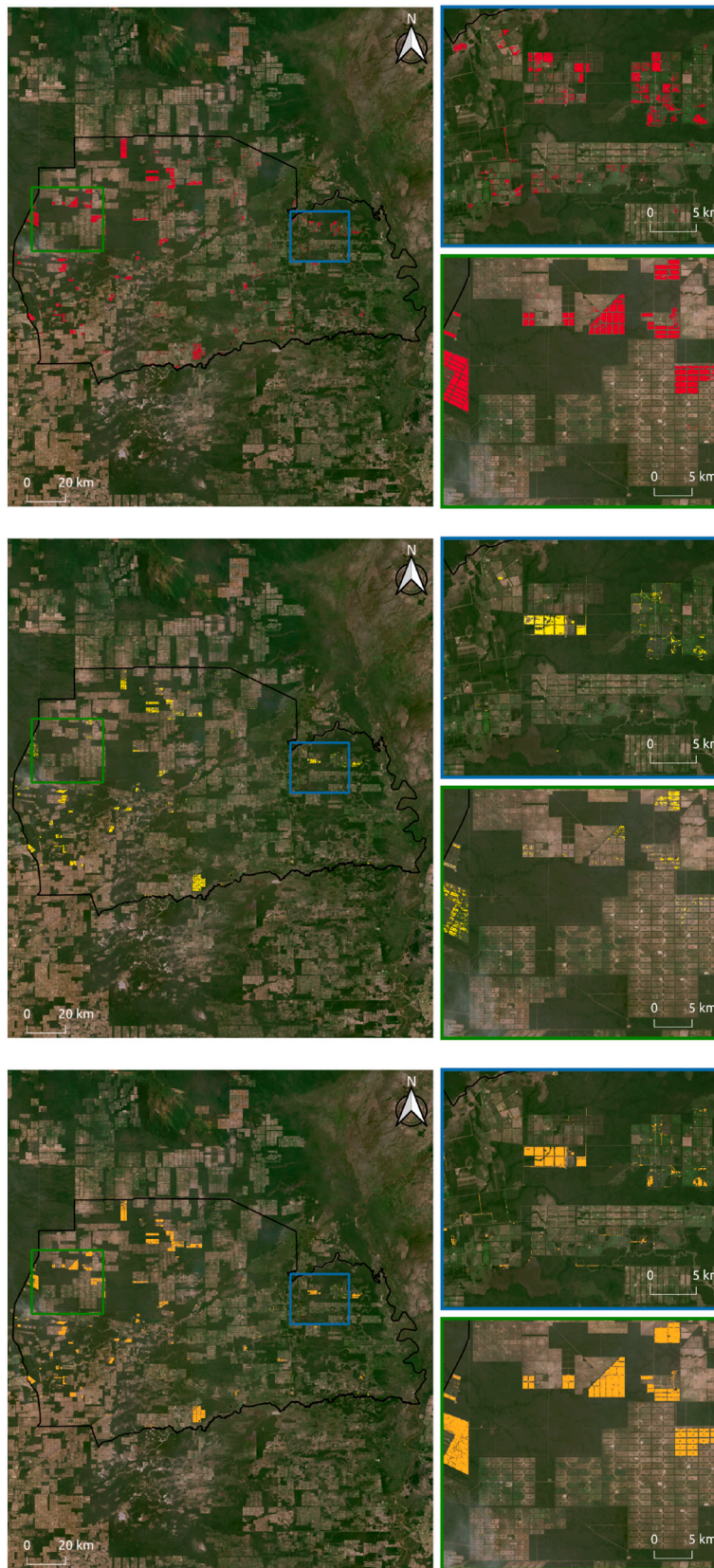
Fig. 9. Visual comparison between our proposed method for alerts in 2020 and 2021 over the Paraguay NRT mapping region (top), Landsat-based GLAD alerts for 2020–2021 (Hansen et al., 2016)(center) and Hansen 2020–2021 forest-cover loss data (Hansen et al., 2013) (bottom).

Fig. 10. Visual comparison between our proposed method for alerts in 2020 and 2021 over the Mozambique NRT mapping region (top), Landsat-based GLAD alerts for 2020–2021 (Hansen et al., 2016)(center) and Hansen 2020–2021 forest-cover loss data (Hansen et al., 2013) (bottom).
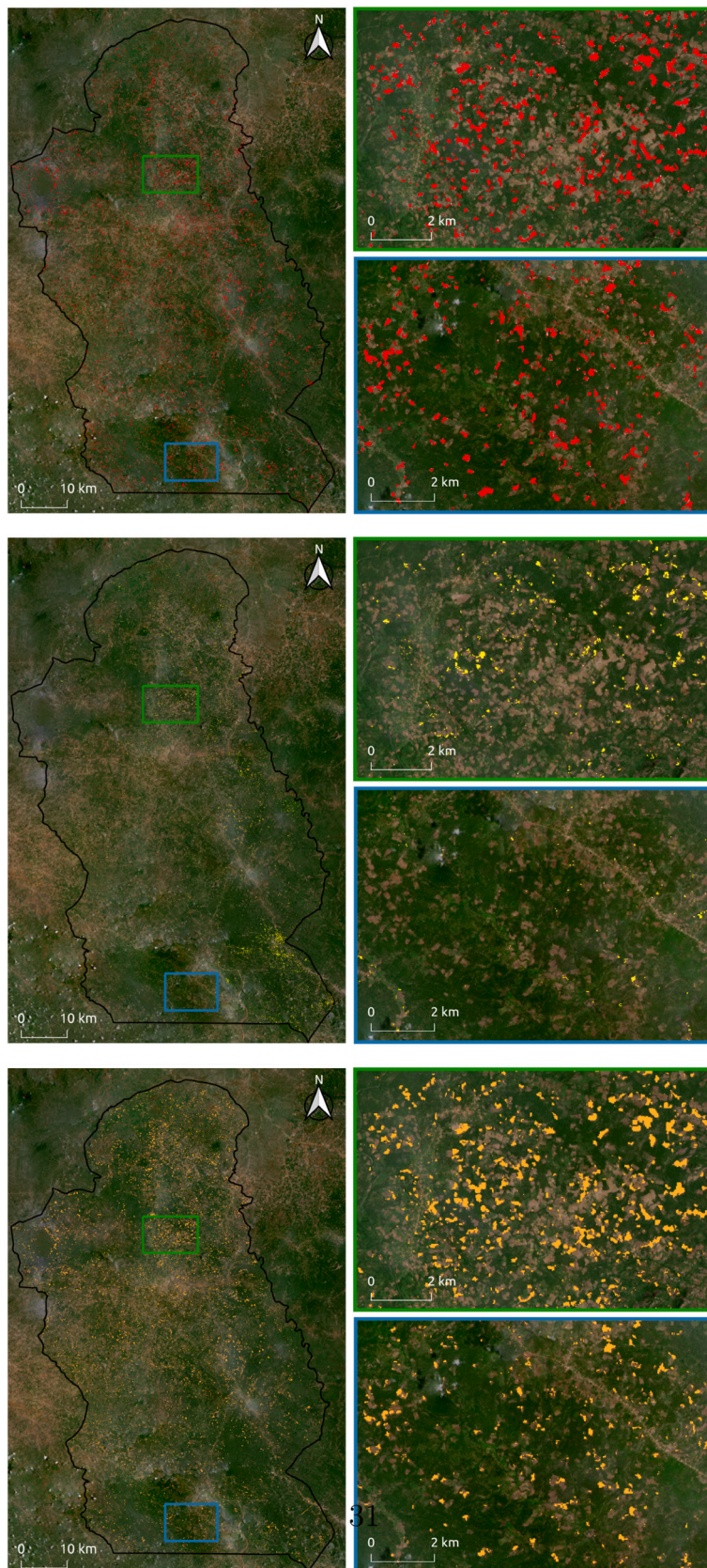
To detect NRT TDF disturbance events, we set a threshold of 0.6 for low confidence alerts and a posterior probability threshold χ of 0.8 to detect the high confidence alerts in both test regions. We used a time window of 90 days to convert the low confidence alerts to a high confidence alerts. Low confidence alerts that were not converted to high confidence alerts within this 90 day period were removed as an alert. Furthermore, low confidence alerts falling behind a threshold value of 0.6 in subsequent acquisitions were discarded. Detected high confidence alerts were not re-detected again in subsequent acquisitions. We discarded detections smaller than 5 (8-connected) pixels at Sentinel-1 scale, therefore, maintaining disturbances at a minimum mapping unit of 0.05 ha. The TDF disturbance alerts were generated over the two test regions for the period 1 January 2020 to 31 December 2021 (Fig. 8).

4.6. Accuracy assessment

We assessed the accuracy of our proposed method in generating the NRT TDF disturbance alert maps by using area-adjusted accuracy assessment suggested in (Olofsson et al., 2014). We generated 1200 sample points using random stratified samples from the detected alerts to derive the accuracy metrics. We allocated 400 sample points in the disturbance stratum, and the remaining 800 points were allocated to the forest baseline and buffer area consisting of 200 m buffer distance from the alert pixels (Olofsson et al., 2020). We used visual inspection of monthly Planet scope image mosaics to derive the ground truth data. We applied the accuracy assessment approach proposed by (Olofsson et al., 2014) to derive the area-adjusted precision (users accuracy), recall (producers accuracy) and F1 score for the forest disturbance alerts. To evaluate the efficacy of the proposed weakly supervised approach, we compared the area-adjusted accuracies of disturbance alerts generated with label harvesting and without label harvesting. To make the comparison fair, we had kept all NRT parameters the same, except the label harvesting. We also compared the accuracies with that of the existing Landsat-based GLAD alert (Hansen et al., 2016) and the Hansen forest-cover loss dataset (Hansen et al., 2013) mapped at Landsat pixel level (0.09 ha MMU) over the test areas.

We also evaluated the differences in timeliness of detections by intersecting confirmed alerts between the proposed method and the Landsat-based GLAD alerts. This comparison was made based on the time when the alert was confirmed as a high confidence alert in both the proposed method and the Landsat-based GLAD alerts.

5. Results

5.1. Label harvesting

To perform label harvesting in the Paraguay test area, we applied a minimum 10% threshold value from each VV and VH image to refine the Hansen Global Forest Change dataset into the initial forest disturbance labels. However, we applied a minimum 35% threshold value of VV and VH image in Mozambique to synthesize the initial forest disturbance data.

To assess the improvement from the weakly supervised label refinement, we trained a DNN model using the unrefined Hansen 2019 forest-cover and Hansen 2020 forest-cover loss. In both the Paraguay and the Mozambique models, the generated alerts achieved a precision, recall and F-1 score of 0.99, 0.61, 0.75 and 0.97, 0.51, 0.66, respectively. The detail precision, recall and F-1 score for the harvested and original Hansen labels is shown in Table 2.

5.2. TDF disturbance detection

The two detailed maps depicted in Fig. 8 show the large scale agriculture derived TDF disturbance in Paraguay and a small holder agriculture and logging driven TDF disturbance in Mozambique. We detected 33.7 kha of disturbance in Paraguay and 14.9 kha of

disturbance in Mozambique test sites, respectively. Detected disturbance events accounted for 1.72% of the study area in Paraguay and 3.12% of the study area in Mozambique, respectively.

5.3. Disturbance alerts accuracy assessment

The area-adjusted accuracy assessment for the disturbance maps in the two test areas yielded consistently high results (Table 2). The area-adjusted precision and recall accuracies for the high confidence alerts in the Paraguay and Mozambique test regions were 99% and 61% and 97.5% and 51%, respectively. These accuracies suggested confident detection of TDF ≥ 0.05 ha. In comparison, the methodology without label harvesting scored significantly lower than the proposed method with a precision of 88% and 13% and 88% and 16% respectively. Similarly, Landsat-based GLAD alerts scored significantly lower than the proposed method in Paraguay and Mozambique, with a precision and recall of 93.5% and 23% and 59% and 6%, respectively. Substantial omission and commission errors were observed in the GLAD alerts compared with the Hansen 2020–2021 forest-cover loss dataset. The Hansen 2020–2021 forest-cover loss dataset performed better than the GLAD alert in Paraguay and Mozambique, with a precision and recall of 95% and 51% and 90% and 40%, respectively. Visual comparisons supported the quantitative results reported in the accuracy assessment (Fig. 9 and Fig. 10).

Assessing the improvement in timeliness showed that the proposed method was detecting disturbances 21 ($\pm$ 18) days earlier than the Landsat-based GLAD alerts in Paraguay, whereas the proposed method detected disturbances 18 ($\pm$ 18) days earlier in Mozambique. We have not determined the absolute mean time lag between our proposed method or the GLAD alert due to inaccuracies associated with extracting these dates from available reference optical and SAR images.

6. Discussion

Our results demonstrated the benefits of automatically harvesting reference labels for NRT TDF disturbance monitoring. They also showed the high quality NRT TDF disturbance detection results that can be derived from applying simple deep learning models. We were able to mitigate TDF seasonality in the Sentinel-1 SAR backscatter signal to detect and monitor disturbances in two different TDF eco-regions with high accuracy.

The Sentinel-1 temporally dense SAR images were important in the rapid detection of TDF disturbance events. The backscatter signal from the C-band radar of Sentinel-1 did not show large variations during the leaf on and off seasons. This characteristic was important to design the proposed method. To avoid false detections in the alerts and preserve the spatial integrity of alerts, the pre-processing steps (Mullissa et al., 2021) in the ARD image generation were crucial.

The selection of features that could represent the dynamics of stable dry forests was found to be another important factor. From this, the minimum 2% of backscatter value was the most important feature. The removal of outliers in the SAR time-series was crucial to estimate the proper feature value for stable forests, as the outliers could bias the estimate. Both polarization states were found to be essential in detecting dry forest disturbance due to the sensitivities of the vegetation to the VH polarization and sensitivity of the VV polarization to bare ground. The stronger contrast in the VV and VH backscatter before and after disturbance led to a better detection of disturbance events. The combination of VV and VH polarization was instrumental in rejecting false detection due to signal anomalies.

The proposed label harvesting showed an alternative cost effective way of reference label generation. The initial filtering and removal of regrowth pixels from the initial reference label guaranteed that the selected pixels corresponded well with a disturbance event that was visible in the SAR images. In addition, the Hansen forest-cover loss data (Hansen et al., 2016) introduced label noise when compared with the

Sentinel-1 SAR images, as optical and SAR images were sensitive to different properties of the forest structure. Therefore, the backscatter filtering avoided these discrepancies in the selection of reference labels. This was clearly shown by the comparison of results applying label harvesting with the original noisy reference labels (Table 2). The intersection of the stable forest dataset (Hansen et al., 2013) with the the DNN predicted stable forest cover improved the confidence of the initial selected forest samples, as the selected disturbance pixels corresponded with disturbance events (such as clear-cut disturbance) that are observable in both SAR and optical images. In the presence of additional forest-cover datasets such as Copernicus dry forest class (Buchhorn et al., 2020), the confidence can be further increased by intersecting these datasets. Overall, the proposed label harvesting method provided a large quantity of high quality reference samples in the dry forest regions and potentially other biomes globally, making it a viable strategy for the preparation of global reference data. The proposed method can also easily be transferred to the humid tropics by adding additional NRT alerts to further improve the confidence of the initial reference dataset.

The application of a DNN architecture improved the deployability of the model in an operational setting. This made the DNN model a suitable candidate to be deployed in an NRT monitoring and evaluation system at a large scale. The trained DNN model was sensitive to the random initialization of parameters. Therefore, the units selected by each hidden layer may fluctuate as a result of this. However, the variation was within ±1 % accuracy in the validation data. The addition of dropout layers in every hidden layer was important to avoid over-fitting to the training data. The models showed slightly higher accuracies due to the correlation between training and test datasets, as they were randomly selected from the same geographic region. However, the high NRT TDF disturbance detection accuracy indicated the same level of performance in a geographically disjointed test region.

The proposed method detected TDF disturbances 21 days (±18 days) in Paraguay and 18 days (±18 days) in Mozambique earlier than than the GLAD alerts; this indicated that the proposed method provides a more rapid detection performance than the optical image based GLAD alert (Hansen et al., 2016), which was mostly effective in detecting disturbances in images with minimal cloud cover conditions. However, some observations in the proposed method have delayed detections due to post-disturbance signal fluctuation, especially in the beginning of the wet season (Fig. 4). However, these alerts were detected once the signal stabilized.

The Sentinel-1 SAR based rapid TDF disturbance detection method that we proposed is unique in that disturbance was detected without deseasonalizing the series, as shown in previous TDF monitoring methods (Reiche et al., 2018). The careful engineering of features, combined with the usage of deep learning models, enabled our proposed method to learn the complex dynamics of an open to closely covered TDF. However, there were some SAR-based NRT THF disturbance alert methods proposed in the literature that relied on change in backscatter during disturbance (Reiche et al., 2021) or detect change in backscatter associated with shadows during disturbance to infer disturbance (Bouvet et al., 2018; Doblas et al., 2022), which worked well for the humid tropics (Doblas Prieto et al., 2023). To extend these methods to TDFs, however, the presence of TDF canopy structure and seasonality remained a challenge. To the best knowledge of the authors, the proposed approach was the first TDF disturbance alert that was designed for monitoring the dry tropics using SAR data.

In summary, our study filled the methodological gap in the application of deep learning to NRT TDF disturbance monitoring using dense Sentinel-1 SAR data. Its simplicity made it easily extendable to other TDF eco-regions and deployable to large-area monitoring applications, which would shed light into the extent of disturbance in a vast portion of tropical forest canopy. Of course, for efficient large-area monitoring computational capability remained a challenge, but the recent advances in the accessibility and affordability of cloud computation technologies showed a promising path ahead (Azzari and Lobell, 2017).

7. Conclusion

We presented rapid forest disturbance mapping for TDF conditions. The availability of uninterrupted supply of dense Sentinel-1 SAR time-series enabled the rapid detection of disturbances within a few weeks after the event actually happened. The methodology proposed a cost-effective method for training and applying machine learning to forest disturbance monitoring. Scaling the proposed approach could help provide new insight into the spatio-temporal dynamics across the dry tropics.

The proposed approach had some remaining limitations of omission of alerts due to moisture, signal fluctuations after disturbance events and regrowth of under-story in open dry forests. In future research, we will focus on addressing the alert omissions shown in the NRT disturbance maps and the deployability and generalization issues associated with deep learning based large-scale NRT TDF disturbance monitoring systems.

Author statement

Aduqna Mullissa: Conceptualization, Methodology, Software, Visualization, Analysis, Writing-original draft preparation.
Johannes Reiche: Conceptualization, Writing-Reviewing and Editing, Fund Acquisition, Supervision.
Martin Herold: Conceptualization, Writing-Reviewing and Editing, Supervision.

Declaration of Competing Interest

The authors declare that they have no known competing financial interests or personal relationships that could have appeared to influence the work reported in this paper.

Data availability

Data will be made available on request.

References

Abadi, M., Barham, P., Chen, J., Chen, Z., Davis, A., Dean, J., Devin, M., Ghemawat, S., Irving, G., Isard, M., 2016. TensorFlow: a system for Large-Scale machine learning. In: 12th USENIX symposium on operating systems design and implementation (OSDI 16), pp. 265–283.

Ahn, J., Kwak, S., 2018. Learning pixel-level semantic affinity with image-level supervision for weakly supervised semantic segmentation. In: Proceedings of the IEEE conference on computer vision and pattern recognition, pp. 4981–4990.

Assunção, J., Gandour, C., Rocha, R., 2013. Deterring deforestation in the brazilian amazon: environmental monitoring and law enforcement. Climate Policy Initiat. 1, 36.

Azzari, G., Lobell, D., 2017. Landsat-based classification in the cloud: an opportunity for a paradigm shift in land cover monitoring. Remote Sens. Environ. 202, 64–74.

Bouvet, A., Mermoz, S., Ballère, M., Koleck, T., Le Toan, T., 2018. Use of the Sar shadowing effect for deforestation detection with sentinel-1 time series. Remote Sens. 10 (8), 1250.

Buchhorn, M., Lesiv, M., Tsendbazar, N.-E., Herold, M., Bertels, L., Smets, B., 2020. Copernicus global land cover layers—collection 2. Remote Sens. 12 (6), 1044.

Chen, N., Tsendbazar, N.-E., Hamunyela, E., Verbesselt, J., Herold, M., 2021. Sub-annual tropical forest disturbance monitoring using harmonized landsat and sentinel-2 data. Int. J. Appl. Earth Obs. Geoinf. 102, 102386.

Daudt, R.Caye, Saux, B.Le, Boulch, A., Gousseau, Y., 2019. Guided anisotropic diffusion and iterative learning for weakly supervised change detection. In: Proceedings of the IEEE/CVF Conference on Computer Vision and Pattern Recognition Workshops, pp. 0–0.

De Sy, V., Herold, M., Achard, F., Asner, G.P., Held, A., Kellndorfer, J., Verbesselt, J., 2012. Synergies of multiple remote sensing data sources for redd+ monitoring. Curr. Opin. Environ. Sustain. 4 (6), 696–706.

Dinerstein, E., Olson, D., Joshi, A., Vynne, C., Burgess, N.D., Wikramanayake, E., Hahn, N., Palminteri, S., Hedao, P., Noss, R., et al., 2017. An ecoregion-based approach to protecting half the terrestrial realm. Bioscience 67 (6), 534–545.

Doblas Prieto, J., Lima, L., Mermoz, S., Bouvet, A., Reiche, J., Watanabe, M., Sant Anna, S., Shimabukuro, Y., 2023. Inter-comparison of optical and Sar-based forest disturbance warning systems in the Amazon shows the potential of combined Sar-optical monitoring. Int. J. Remote Sens. 44 (1), 59–77.

Doblas, J., Reis, M.S., Belluzzo, A.P., Quadros, C.B., Moraes, D.R., Almeida, C.A., Maurano, L.E., Carvalho, A.F., Sant'Anna, S.J., Shimabukuro, Y.E., 2022. Deter-r: An operational near-real time tropical forest disturbance warning system based on sentinel-1 time series analysis. Remote Sens 14 (15), 3658.

Gorelick, N., Hancher, M., Dixon, M., Ilyushchenko, S., Thau, D., Moore, R., 2017. Google earth engine: planetary-scale geospatial analysis for everyone. Remote Sens. Environ. 202, 18–27.

Hampel, F.R., 1974. The influence curve and its role in robust estimation. J. Am. Stat. Assoc. 69 (346), 383–393.

Hamunyela, E., Verbesselt, J., Herold, M., 2016. Using spatial context to improve early detection of deforestation from landsat time series. Remote Sens. Environ. 172, 126–138.

Hansen, M.C., Potapov, P.V., Moore, R., Hancher, M., Turubanova, S.A., Tyukavina, A., Thau, D., Stehman, S.V., Goetz, S.J., Loveland, T.R., et al., 2013. High-resolution global maps of 21st-century forest cover change. Science 342 (6160), 850–853.

Hansen, M.C., Krylov, A., Tyukavina, A., Potapov, P.V., Turubanova, S., Zutta, B., Ifo, S., Margono, B., Stolle, F., Moore, R., 2016. Humid tropical forest disturbance alerts using Landsat data. Environ. Res. Lett. 11 (3), 034008.

Hartung, M., Carreño-Rocabado, G., Peña-Claros, M., van der Sande, M.T., 2021. Tropical dry forest resilience to fire depends on fire frequency and climate. Front. Forests Global Change 4, 755104.

Hoekman, D.H., Reiche, J., 2015. Multi-model radiometric slope correction of Sar images of complex terrain using a two-stage semi-empirical approach. Remote Sens. Environ. 156, 1–10.

Hoekman, D., Kooij, B., Quiñones, M., Vellekoop, S., Carolita, I., Budhiman, S., Arief, R., Roswintiarti, O., 2020. Wide-area near-real-time monitoring of tropical forest degradation and deforestation using sentinel-1. Remote Sens. 12 (19), 3263.

Huang, Z., Wang, X., Wang, J., Liu, W., Wang, J., 2018. Weakly-supervised semantic segmentation network with deep seeded region growing. In: Proceedings of the IEEE conference on computer vision and pattern recognition, pp. 7014–7023.

Ioffe, S., Szegedy, C., 2015. Batch normalization: Accelerating deep network training by reducing internal covariate shift. In: International conference on machine learning, PMLR, pp. 448–456.

Janzen, D.H., 1988. Tropical dry forests. Biodiversity 15, 130–137.

Joshi, N., Baumann, M., Ehammer, A., Fensholt, R., Grogan, K., Hostert, P., Jepsen, M.R., Kuemmerle, T., Meyfroidt, P., Mitchard, E.T., et al., 2016. A review of the application of optical and radar remote sensing data fusion to land use mapping and monitoring. Remote Sens. 8 (1), 70.

Kingma, D.P., Ba, J., 2014. Adam: A method for stochastic optimization, arXiv preprint arXiv:1412.6980.

Laurin, G.V., Liesenberg, V., Chen, Q., Guerriero, L., Del Frate, F., Bartolini, A., Coomes, D., Wilebore, B., Lindsell, J., Valentini, R., 2013. Optical and Sar sensor synergies for forest and land cover mapping in a tropical site in west africa. Int. J. Appl. Earth Obs. Geoinf. 21, 7–16.

Lee, J.-S., 1981. Speckle analysis and smoothing of synthetic aperture radar images. Comput. Graph. Image Process. 17 (1), 24–32.

Lewis, S.L., Lloyd, J., Sitch, S., Mitchard, E.T., Laurance, W.F., 2009. Changing ecology of tropical forests: evidence and drivers. Annu. Rev. Ecol. Evol. Syst. 40, 529–549.

Li, L., Jamieson, K., DeSalvo, G., Rostamizadeh, A., Talwalkar, A., 2017. Hyperband: a novel bandit-based approach to hyperparameter optimization. J. Machine Learn. Res. 18 (1), 6765–6816.

Liu, Z., Peng, C., Work, T., Candau, J.-N., DesRochers, A., Kneeshaw, D., 2018. Application of machine-learning methods in forest ecology: recent progress and future challenges. Environ. Rev. 26 (4), 339–350.

Liu, R., Kuffer, M., Persello, C., 2019. The temporal dynamics of slums employing a CNN-based change detection approach. Remote Sens. 11 (23), 2844.

Lynch, J., Maslin, M., Balzter, H., Sweeting, M., 2013. Choose satellites to monitor deforestation. Nature 496 (7445), 293–294.

Miles, L., Newton, A.C., DeFries, R.S., Ravilious, C., May, I., Blyth, S., Kapos, V., Gordon, J.E., 2006. A global overview of the conservation status of tropical dry forests. J. Biogeogr. 33 (3), 491–505.

Mullissa, A., Vollrath, A., Odongo-Braun, C., Slagter, B., Balling, J., Gou, Y., Gorelick, N., Reiche, J., 2021. Sentinel-1 Sar backscatter analysis ready data preparation in Google Earth Engine. Remote Sens. 13 (10), 1954.

Mullissa, A.G., Reiche, J., Saatchi, S., 2023. Seasonal forest disturbance detection using sentinel-1 sar sentinel-2 optical time-series data and transformers. In: IGARSS 2023-2023 IEEE International Geoscience and Remote Sensing Symposium, IEEE.

Murphy, P.G., Lugo, A.E., 1995. In: Dry Forests of Central America and the Caribbean, Seasonally Dry Tropical Forests. Cambridge University Press, Cambridge, pp. 9–34.

Nazerali, S., Chauque, A., 2023. A contribution to mozambique's biodiversity offsetting system: framework to assess the ecological condition of miombo woodlands.

O'Malley, T., Bursztein, E., Long, J., Chollet, F., Jin, H., Invernizzi, L., 2019. Kerastuner. https://github.com/keras-team/keras-tuner.

Olofsson, P., Foody, G.M., Herold, M., Stehman, S.V., Woodcock, C.E., Wulder, M.A., 2014. Good practices for estimating area and assessing accuracy of land change. Remote Sens. Environ. 148, 42–57.

Olofsson, P., Arévalo, P., Espejo, A.B., Green, C., Lindquist, E., McRoberts, R.E., Sanz, M. J., 2020. Mitigating the effects of omission errors on area and area change estimates. Remote Sens. Environ. 236, 111492.

Pacheco-Pascagaza, A.M., Gou, Y., Louis, V., Roberts, J.F., Rodríguez-Veiga, P., da Conceição Bispo, P., Espírito-Santo, F.D., Robb, C., Upton, C., Galindo, G., et al., 2022. Near real-time change detection system using sentinel-2 and machine learning: a test for Mexican and Colombian forests. Remote Sens. 14 (3), 707.

Pearson, T.R., Brown, S., Murray, L., Sidman, G., 2017. Greenhouse gas emissions from tropical forest degradation: an underestimated source. Carbon Balance Manag. 12, 1–11.

Portillo-Quintero, C.A., Sánchez-Azofeifa, G.A., 2010. Extent and conservation of tropical dry forests in the Americas. Biol. Conserv. 143 (1), 144–155.

Quegan, S., Yu, J.J., 2001. Filtering of multichannel Sar images. IEEE Trans. Geosci. Remote Sens. 39 (11), 2373–2379.

Reiche, J., De Bruin, S., Hoekman, D., Verbesselt, J., Herold, M., 2015. A bayesian approach to combine Landsat and alos palsar time series for near real-time deforestation detection. Remote Sens. 7 (5), 4973–4996.

Reiche, J., Verbesselt, J., Hoekman, D., Herold, M., 2015. Fusing landsat and Sar time series to detect deforestation in the tropics. Remote Sens. Environ. 156, 276–293.

Reiche, J., Hamunyela, E., Verbesselt, J., Hoekman, D., Herold, M., 2018. Improving near-real time deforestation monitoring in tropical dry forests by combining dense sentinel-1 time series with landsat and alos-2 palsar-2. Remote Sens. Environ. 204, 147–161.

Reiche, J., Mullissa, A., Slagter, B., Gou, Y., Tsendbazar, N.-E., Odongo-Braun, C., Vollrath, A., Weisse, M.J., Stolle, F., Pickens, A., et al., 2021. Forest disturbance alerts for the Congo basin using sentinel-1. Environ. Res. Lett. 16 (2), 024005.

Rosenqvist, A., Shimada, M., Watanabe, M., 2004. Alos palsar: Technical outline and mission concepts. In: 4th International Symposium on Retrieval of Bio-and Geophysical Parameters from SAR Data for Land Applications. Innsbruck, Austria, pp. 1–7.

Sannier, C., McRoberts, R.E., Fichet, L.-V., Makaga, E.M.K., 2014. Using the regression estimator with Landsat data to estimate proportion forest cover and net proportion deforestation in Gabon. Remote Sens. Environ. 151, 138–148.

Solórzano, J.V., Gao, Y., 2022. Forest disturbance detection with seasonal and trend model components and machine learning algorithms. Remote Sens. 14 (3), 803.

Souza Jr., C.M., Siqueira, J.V., Sales, M.H., Fonseca, A.V., Ribeiro, J.G., Numata, I., Cochrane, M.A., Barber, C.P., Roberts, D.A., Barlow, J., 2013. Ten-year Landsat classification of deforestation and forest degradation in the Brazilian Amazon. Remote Sens. 5 (11), 5493–5513.

Torres, R., Snoeij, P., Geudtner, D., Bibby, D., Davidson, M., Attema, E., Potin, P., Rommen, B., Floury, N., Brown, M., et al., 2012. Gmes sentinel-1 mission. Remote Sens. Environ. 120, 9–24.

Ulaby, F.T., Moore, R.K., Fung, A.K., 1986. Microwave remote sensing: Active and passive. volume 3-from theory to applications.

Verbesselt, J., Hyndman, R., Newnham, G., Culvenor, D., 2010. Detecting trend and seasonal changes in satellite image time series. Remote Sens. Environ. 114 (1), 106–115.

Verhegghen, A., Kuzelova, K., Syrris, V., Eva, H., Achard, F., 2022. Mapping canopy cover in African dry forests from the combined use of sentinel-1 and sentinel-2 data: application to Tanzania for the year 2018. Remote Sens. 14 (6), 1522.

Vollrath, A., Mullissa, A., Reiche, J., 2020. Angular-based radiometric slope correction for sentinel-1 on google earth engine. Remote Sens. 12 (11), 1867.

Wang, Q., Zhang, X., Chen, G., Dai, F., Gong, Y., Zhu, K., 2018. Change detection based on faster r-cnn for high-resolution remote sensing images. Remote Sens. Lett. 9 (10), 923–932.

Wang, H., Zhao, X., Zhang, X., Wu, D., Du, X., 2019. Long time series land cover classification in China from 1982 to 2015 based on bi-lstm deep learning. Remote Sens. 11 (14), 1639.

Wang, Y., Zhang, J., Kan, M., Shan, S., Chen, X., 2020. Self-supervised equivariant attention mechanism for weakly supervised semantic segmentation. In: Proceedings of the IEEE/CVF Conference on Computer Vision and Pattern Recognition, pp. 12275–12284.

Watanabe, M., Koyama, C.N., Hayashi, M., Nagatani, I., Tadono, T., Shimada, M., 2021. Refined algorithm for forest early warning system with alos-2/palsar-2 scansar data in tropical forest regions. Remote Sens. Environ. 265, 112643.

Wei, Y., Liang, X., Chen, Y., Shen, X., Cheng, M.-M., Feng, J., Zhao, Y., Yan, S., 2016. Stc: a simple to complex framework for weakly-supervised semantic segmentation. IEEE Trans. Pattern Anal. Mach. Intell. 39 (11), 2314–2320.

Wheeler, D., Hammer, D., Kraft, R., Steele, A., 2014. Satellite-based forest clearing detection in the Brazilian Amazon.

14

Ye, L., Gao, L., Marcos-Martinez, R., Mallants, D., Bryan, B.A., 2019. Projecting australia's forest cover dynamics and exploring influential factors using deep learning. Environ. Model Softw. 119, 407–417.

Zheng, A., Casari, A., 2018. Feature engineering for machine learning: Principles and techniques for data scientists. O'Reilly Media, Inc.", ".

Zhong, L., Hu, L., Zhou, H., 2019. Deep learning based multi-temporal crop classification. Remote Sens. Environ. 221, 430–443.

Zhou, Z.-H., 2018. A brief introduction to weakly supervised learning. Natl. Sci. Rev. 5 (1), 44–53.

Zhou, X., Fu, Y., Zhou, L., Li, B., Luo, Y., 2013. An imperative need for global change research in tropical forests. Tree Physiol. 33 (9), 903–912.

Zhu, Z., Woodcock, C.E., Olofsson, P., 2012. Continuous monitoring of forest disturbance using all available landsat imagery. Remote Sens. Environ. 122, 75–91.